

# Properties of the double $\beta$ model for intracluster gas

Yan-Jie Xue and Xiang-Ping Wu

*Beijing Astronomical Observatory and National Astronomical Observatories, Chinese Academy of Sciences, Beijing 100012, China*

Accepted 2000 June 8. in original form 1999 September 29

## ABSTRACT

We present an extensive study of the double  $\beta$  model for the X-ray surface brightness profiles of clusters, and derive analytically the gas density and total masses of clusters under the hydrostatic equilibrium hypothesis. It is shown that the employment of the double  $\beta$  model instead of the conventional single  $\beta$  model can significantly improve the goodness of fit to the observed X-ray surface brightness profiles of clusters, which will in turn lead to a better determination of the gas and total mass distributions in clusters. In particular, the observationally fitted  $\beta$  parameter for the extended component in a double  $\beta$  model may become larger. This opens a new possibility of resolving the long-standing  $\beta$  discrepancy for clusters. Using an ensemble of 33 ROSAT PSPC observed clusters drawn from the Mohr, Mathiesen & Evrard (1999) sample, we find that the asymptotic value of  $\beta_{fit}$  is  $0.83 \pm 0.33$  at large radii, consistent with both the average spectroscopic parameter  $\beta_{spec} = 0.78 \pm 0.37$  and the result given by numerical simulations.

**Key words:** galaxies: clusters: general — intergalactic medium — X-rays: galaxies

## 1 INTRODUCTION

Since the pioneering work of Cavaliere & Fusco-Femiano (1976), the  $\beta$  model has been widely adopted in the fitting of the X-ray surface brightness profiles of galaxy clusters. In particular, despite the difference in the core radius there is a striking similarity between the X-ray surface brightness distribution predicted by the universal density profile as the underlying gravitational potential of a cluster and the conventional  $\beta$  model (Makino, Sasaki & Suto 1998). Yet, it has been realized for many years that a single  $\beta$  model is inaccurate and also not self-consistent. First, it fails to represent the central excess emission associated with the cooling flows seen in many clusters. Second, the X-ray luminosity is divergent for  $\beta < 0.5$  so that an arbitrary cutoff radius should be introduced (e.g. Henry & Henriksen 1986). Third, an increasing temperature with cluster radius is required for  $\beta < 2/3$  if the asymptotic baryon fraction of cluster at large radii should reach a universal value defined by the Big Bang Nucleosynthesis (Wu & Xue 2000). Finally, the well-known  $\beta$  discrepancy (e.g. Bahcall & Lubin 1994) may also arise from the employment of a single  $\beta$  model. Namely, the slope of gas radial profile described by a single  $\beta$  model is systematically smaller than that required by the equipartition between specific kinetic energy in galaxies and that in gas.

Regardless of its simplification, the second  $\beta$  model has been formally adopted by a number of authors in recent years to represent the excess X-ray emission in the central cores of cooling flow clusters (e.g. Ikebe et al. 1996; 1999;

Xu et al. 1998; Mohr, Mathiesen & Evrard 1999, MME hereafter). An immediate consequence of fitting the X-ray surface brightness profile with a double  $\beta$  model instead of a single  $\beta$  model is that the resultant  $\beta$  parameters in the two components may both become larger. In particular, it seems that the  $\beta$  parameter for the extended component can often be greater than  $2/3$ . Therefore, there is a possibility that a double  $\beta$  model may allow one to resolve all the above puzzles associated with a single  $\beta$  model. Moreover, in the conventional single  $\beta$  model fit, some of the observed data points in the central regions of the cooling flow clusters should be omitted in order to obtain an acceptable fit (e.g. Jones & Forman 1984), while in some cases, the sizes of the excluded regions are not at all obvious. The introduction of a double  $\beta$  model thus provides a way to quantitatively describe the central excess emission. In fact, as will be shown in this paper, our understanding of some properties of clusters such as the determinations of gas density and dynamical mass is closely connected to the issue as to whether or not the central narrow component is properly taken into account. On the other hand, there have been increasing studies both theoretically and observationally on the possibility that intracluster gas is multiphase (Nulsen 1986; White & Fabian 1995; Gunn & Thomas 1996; Nagai, Sulkanen & Evrard 2000; Buote 2000, etc.), among which the detection of excess of low-energy photons in X-ray spectra relative to the average X-ray temperature in some clusters gives a convincing support to the presence of a cold gas component either concentrated in the central core or distributed

arXiv:astro-ph/0006131v1 9 Jun 2000

over the entire cluster. A double  $\beta$  model may correspond to the simplest case for multiphase medium, and therefore a detailed study of its properties will be helpful for our further investigation of the complex and multiphase intracluster gas.

In this paper, we present the gas distribution inferred from a double  $\beta$  model (section 2.1) and the total cluster mass under the assumption that the two-phase gas is in hydrostatic equilibrium with the underlying gravitational potential of the cluster (section 2.2). We demonstrate the difference in the cluster properties characterized by a single and double  $\beta$  model using two strong cooling flow clusters, A2597 and A2390 (section 3). Because the sharp peak in the central X-ray emission can be quantitatively described by the second  $\beta$  model, we will be able to estimate more accurately the cluster mass enclosed within the central core and compare with that derived from strong gravitational lensing. We will examine whether the double  $\beta$  model corrected X-ray mass can be reconciled with the strong lensing result (e.g. Wu & Fang 1997). Finally, as a consequence of adopting a double  $\beta$  model fit, the  $\beta$  parameters in the two components may both become larger than the value in a single  $\beta$  model fit. We will study the possibility of resolving the well-known  $\beta$  discrepancy, using a sample of 33 clusters drawn from the recent work of MME. Throughout this paper we assume  $H_0 = 50 \text{ km s}^{-1} \text{ Mpc}^{-1}$  and  $\Omega_0 = 1$ .

## 2 THE MODEL

### 2.1 GAS DISTRIBUTION

If we assume that the intracluster gas has two-phases with different electron temperatures  $T_i$ , where and also hereafter the subscript number ( $i = 1, 2$ ) refers to the two-phases, the X-ray emission per unit volume in an energy band from  $E_1$  to  $E_2$ , according to thermal bremsstrahlung, is

$$\frac{dL_x}{dV} = \sum_i \alpha(T_i) n_{ei} \sum_{z,Z} N_{Z,z} z^2 g_i \quad (1)$$

where

$$\alpha(T_i) = \frac{2^4 e^6}{3m_e \hbar c^2} \left( \frac{2\pi k T_i}{3m_e c^2} \right)^{1/2}, \quad (2)$$

and

$$g_i = \int_{E_1}^{E_2} \bar{g}_{ff}(T_i, \nu) e^{-\frac{h\nu}{kT_i}} d\left(\frac{h\nu}{kT_i}\right), \quad (3)$$

in which  $n_e$  is the electron number density,  $N_{Z,z}$  is the ion number density with atomic number  $Z$  and effective charges  $z$ , and  $\bar{g}_{ff}$  is the Guant factor of the free-free emission. We define the average electron weight  $\mu_{ei}$  (or  $\mu_e$ ) as

$$\mu_{ei} n_{ei} = \mu_e n_e = \sum_{z,Z} N_{Z,z} z^2 \quad (4)$$

where  $n_e = \sum_i n_{ei}$  is the total electron number density, so that

$$\sum_i \frac{1}{\mu_{ei}} = \frac{1}{\mu_e}. \quad (5)$$

In particular, if intracluster gas is assumed to have the cosmic primordial abundances of hydrogen and helium, then

$\mu_e = 2/(1+X)$  with  $X$  being the primordial hydrogen mass fraction  $X = 0.768$ .

Suppose that the two-phase emission gives rise to, correspondingly, the two components in the observed X-ray surface brightness profile described by a double  $\beta$  model:

$$S(r) = \sum_i S_{0i} \left( 1 + \frac{r^2}{r_{ci}^2} \right)^{-3\beta_i + 0.5}. \quad (6)$$

By inverting  $S(r)$  and comparing with eq.(1), we have (e.g. Cowie, Henriksen & Mushotzky 1987)

$$\mu_{ei}(0) n_{ei}^2(0) = \frac{4\pi^{1/2}}{\alpha(T_i) g_i} \frac{\Gamma(3\beta_i)}{\Gamma(3\beta_i - \frac{1}{2})} \frac{S_{0i}}{r_{ci}}, \quad (7)$$

and

$$\mu_{ei} n_{ei}^2 = \mu_{ei}(0) n_{ei}^2(0) \left( 1 + \frac{r^2}{r_{ci}^2} \right)^{-3\beta_i}. \quad (8)$$

Eliminating  $\mu_{ei}$  in the above equations in terms of eqs.(4) and (5), we can get the electron number densities for the two components as well as the combined electron number density  $n_e$

$$\frac{n_{ei}}{n_{ei}(0)} = \left( 1 + \frac{r^2}{r_{ci}^2} \right)^{-\frac{3\beta_i}{2}} \left[ \frac{n_{e0} \left( 1 + \frac{r^2}{r_{ci}^2} \right)^{-3\beta_i}}{\sum_i n_{ei}(0) \left( 1 + \frac{r^2}{r_{ci}^2} \right)^{-3\beta_i}} \right]^{1/2}, \quad (9)$$

or

$$n_{ei} = \left( \frac{n_{e0}}{n_e} \right) \tilde{n}_{ei}, \quad (10)$$

and

$$n_e = \sum_i n_{ei} = \left[ n_{e0} \sum_i \tilde{n}_{ei} \right]^{1/2}, \quad (11)$$

in which

$$\tilde{n}_{ei} \equiv n_{ei}(0) \left( 1 + \frac{r^2}{r_{ci}^2} \right)^{-3\beta_i}. \quad (12)$$

Note that although eq.(11) can be formally written as  $n_{gas} = [n_{gas1}^2 + n_{gas2}^2]^{1/2}$ , which has been adopted in some recent work (e.g. Reiprich & Böhringer 1999), the determination of the central gas density for each component ( $n_{gas1}$  or  $n_{gas2}$ ) described by a single  $\beta$  model is dependent on both components of  $S(r)$ . In terms of eq.(7), the central electron number density,  $n_{ei}(0)$ , is related to the observationally fitted central surface brightness  $S_{0i}$  through

$$n_{ei}^2(0) = \frac{4\pi^{1/2}}{\alpha(T_i) g_i \mu_e} \frac{\Gamma(3\beta_i)}{\Gamma(3\beta_i - \frac{1}{2})} \frac{S_{0i}}{r_{ci}} A_{ij}, \quad (13)$$

in which

$$\frac{1}{A_{ij}} = 1 + \frac{S_{0j} r_{ci} g_i}{S_{0i} r_{cj} g_j} \left( \frac{T_i}{T_j} \right)^{1/2} \frac{\Gamma(3\beta_j)}{\Gamma(3\beta_i)} \frac{\Gamma(3\beta_i - \frac{1}{2})}{\Gamma(3\beta_j - \frac{1}{2})}, \quad (14)$$

where and also hereafter  $j = 1, 2$  and  $j \neq i$ . Of course, one can also estimate  $n_{ei}(0)$  using the total X-ray luminosity  $L_x$  of the cluster (eq.[1]). For example, in the case of isothermal gas distributions for the two-phase gas we have

$$n_{ei}^2(0) = \frac{L_x A_{ij} B_{ij}}{\pi^{3/2} \alpha(T_i) g_i \mu_e r_{ci}^3} \frac{\Gamma(3\beta_i)}{\Gamma(3\beta_i - \frac{3}{2})}, \quad (15)$$

where

$$\frac{1}{B_{ij}} = 1 + \frac{S_{0j} r_{cj}^2}{S_{0i} r_{ci}^2} \frac{3\beta_i - \frac{3}{2}}{3\beta_j - \frac{3}{2}}. \quad (16)$$

Apparently, the total X-ray luminosity can be estimated simply from

$$L_x = \sum_i \frac{4\pi^2 r_{ci}^2 S_{0i}}{3\beta_i - \frac{3}{2}}. \quad (17)$$

## 2.2 CLUSTER MASS

The total mass in gas within a sphere of radius  $r$  is

$$M_{gas}(r) = 4\pi\mu_e m_p n_{e0} \int_0^r \left[ \frac{1}{n_{e0}} \sum_i \tilde{n}_{ei}(r) \right]^{1/2} r^2 dr, \quad (18)$$

If the X-ray emitting gas is in hydrostatic equilibrium with the underlying gravitational potential of the cluster, the total dynamical mass within  $r$  is

$$M(r) = -\frac{r^2}{G\mu_e m_p n_e} \sum_i \frac{d(n_i k T_i)}{dr}, \quad (19)$$

in which  $n_i$  is the total particle number density for the  $i$ th-phase gas. If the abundances of hydrogen and helium for a single-phase gas are assumed to remain unchanged over the whole cluster, we have  $n_i = \mu_{si} n_{ei}$ , where  $\mu_{si}$  is a proportionality coefficient. If the two-phases both have the cosmic mixed-abundances of hydrogen and helium,  $\mu_{si} = 1.934$ . Next, we assume a polytropic equation of state for each single-phase gas, namely,  $T_i = T_{i0} [n_{ei}/n_{ei}(0)]^{\gamma_i - 1}$ . In this case, eq.(19) can be written to be

$$M(r) = -\sum_i \frac{\gamma_i k T_{i0} r}{G\mu_i m_p} \left( \frac{n_{ei}}{n_{ei}(0)} \right) \left( \frac{n_{ei}}{n_e} \right) \left( \frac{d \ln n_{ei}}{d \ln r} \right), \quad (20)$$

where  $\mu_i = \mu_e / \mu_{si}$ . A straightforward computation using the electron number density found in the above subsection yields

$$M(r) = \sum_{i,j} M_i(r) \left( \frac{n_{ei}}{n_e} \right) \cdot \left[ 1 + \left( 1 - \frac{\beta_j}{\beta_i} \frac{r^2 + r_{ci}^2}{r^2 + r_{cj}^2} \right) \frac{\tilde{n}_{ej}}{\tilde{n}_{ei} + \tilde{n}_{ej}} \right], \quad (21)$$

where  $M_i(r)$  is the total cluster mass determined by assuming that the X-ray emission is from a single-phase medium described by a single  $\beta$  model:

$$M_i(r) = 3\beta_i \gamma_i \frac{k T_{i0} r}{G\mu_i m_p} \frac{r^2}{r^2 + r_{ci}^2} \left( \frac{n_{ei}(r)}{n_{ei}(0)} \right)^{\gamma_i - 1}. \quad (22)$$

It is easy to show that eq.(21) reduces to the form of eq.(22) if the two-phase gas components are assumed to be identical or the second component vanishes.

## 3 APPLICATION TO X-RAY CLUSTERS

### 3.1 A2579

We first choose a typical cooling flow cluster, A2579, to demonstrate how a double  $\beta$  model works. A2579 has been extensively studied by Sarazin & McNamara (1997). They

showed that the merged ROSAT HRI and PSPC surface brightness profile  $S(x)$  cannot be fitted by a single  $\beta$  model unless the data points within the central region of radius of 0.18 Mpc are removed. Meanwhile, the core radius has not been well constrained due to the presence of the centrally peaked X-ray emission, and the gas and total masses within the central region derived from the deconvolved gas density are apparently larger than those obtained from the best-fit single  $\beta$  model. We now make an attempt to fit the same data set  $S(x)$  using a double  $\beta$  model (eq.[6]). Fig.1 displays the observed and our best-fit X-ray surface brightness profiles of A2579. It turns out that the goodness of the fit has been significantly improved when a double  $\beta$  model is applied to the entire data points, yielding  $\chi^2/\nu = 41.16/26$ . Recall that the minimum  $\chi^2/\nu$  is 59.99 for 29 d.o.f in a single  $\beta$  model fitting (Sarazin & McNamara 1997). The best-fit values of the  $\beta$  parameter and core radius for the narrow and extended components are  $(\beta_1, r_{c1}) = (0.70 \pm 0.32, 0.047 \pm 0.016 \text{ Mpc})$  and  $(\beta_2, r_{c2}) = (0.66 \pm 0.03, 0.15 \pm 0.05 \text{ Mpc})$ , respectively. Note that our fitted  $\beta$  parameter for the extended component is close to the value (0.64) obtained by Sarazin & McNamara (1997) who have excluded the central cooling flow region. Alternatively, the two components in our double  $\beta$  model exhibit similar  $\beta$  values. The same situation has been known for A1795 (Xu et al. 1998), while MME assumed the two components of a double  $\beta$  model to have the same  $\beta$  in their analysis of 45 nearby clusters. We have also tried the double  $\beta$  fit by correcting the PSF of the ROSAT HRI with a FWHM of 4 arcseconds. This results in a slightly smaller core radius for the narrow component  $(\beta_1, r_{c1}) = (0.67 \pm 0.33, 0.041 \pm 0.016 \text{ Mpc})$ , while the extended component remains almost unchanged. Finally, we have compared in Fig.1 the electron number density given by the deprojection technique with that calculated from our best-fit double  $\beta$  model assuming  $T_1 = 2.0 \text{ keV}$  and  $T_2 = 4.34 \text{ keV}$  for the narrow and extended components, respectively. The agreement between the two results is good with  $\chi^2 = 41.06$  for 32 d.o.f. although the very central point shows a deviation from the expectation of our double  $\beta$  model. Note that the temperature of the cluster, especially the outer cluster, is poorly constrained. Our choice of  $T_1$  and  $T_2$  is simply based on the single temperature model fits by Sarazin & McNamara (1997) to the ROSAT PSPC spectra of the core region (0.1 Mpc) and the outer cluster (0.25–1 Mpc), respectively.

### 3.2 A2390

The reason why we choose A2390 for a further demonstration of the double  $\beta$  model is as follows: First, a single  $\beta$  model fails to fit the merged ROSAT HRI and PSPC surface brightness profile  $S(x)$  of the cluster, which has been well observed out to a radius of  $\sim 2 \text{ Mpc}$  (Böhringer et al. 1998); Second, the mass distribution of the cluster has been mapped with the weak lensing technique (Squires et al. 1996). It deserves to be examined whether the cluster mass derived from a double  $\beta$  model can be reconciled with the weak lensing result. The latter is believed to provide a reliable mass estimate, independently of the cluster matter contents and their dynamical states. Third, none of the suggested models in literature based on the fitting of  $S_x$  have reproduced the mass profile given by the weak lensing analy-

sis (Böhringer et al. 1998). In Fig.2 we plot the X-ray surface brightness profile of A2390 observed from the ROSAT HRI and PSPC (Böhringer et al. 1998), along with a single and double  $\beta$  model fitting. The best-fit parameters are  $(\beta, r_c) = (0.56 \pm 0.01, 0.11 \pm 0.01 \text{ Mpc})$  for a single  $\beta$  model with  $\chi^2/\nu = 209.08/40$ , and  $(\beta_1, r_{c1}) = (0.92 \pm 0.22, 0.46 \pm 0.16 \text{ Mpc})$  and  $(\beta_2, r_{c2}) = (0.51 \pm 0.01, 0.046 \pm 0.010 \text{ Mpc})$  for a double  $\beta$  model with  $\chi^2/\nu = 52.48/37$ , respectively. Indeed, a single  $\beta$  model fit is not acceptable. Böhringer et al. (1998) obtained a good fit by introducing a Gaussian peak plus a single  $\beta$  model. Our double  $\beta$  model does provide a significantly reduced  $\chi^2$  fit to the entire data points although the two components appear to be unusual in shape. Because A2390 is located at moderate redshift ( $z = 0.228$ ), we may need to consider whether the core radius is overestimated in the above fitting due to the PSF of the ROSAT HRI. We repeat the double  $\beta$  model fitting using a PSF with a FWHM of 4 arcseconds. The best fit parameters become  $(\beta_1, r_{c1}) = (0.98 \pm 0.12, 0.49 \pm 0.08 \text{ Mpc})$  and  $(\beta_2, r_{c2}) = (0.50 \pm 0.01, 0.035 \pm 0.005 \text{ Mpc})$ . Indeed, for the second component the core radius is apparently reduced, while the  $\beta$  parameter remains roughly the same.

Now, we calculate the projected cluster mass within radius  $r$ . The major uncertainty here is the X-ray temperatures for the two components of the double  $\beta$  model. The presence of the cooling flow may lead to an underestimate of the overall temperature of the cluster. The reported temperature of the cluster in the literature ranges from the average value  $7.7_{-0.98}^{+1.29}$  keV over the cluster (Rizza et al. 1998) to the cooling flow corrected value  $23.09 \pm 35.12$  keV (White 2000). Moreover, there is an apparent discrepancy between the ROSAT PSPC and ASCA GIS measured temperatures within the central region of the cluster. In the following we first adopt the two-temperature model of Böhringer et al. (1998), which consists of a narrow, low-temperature component with  $T_1$  and an extended, high-temperature one with  $T_2$ . The projected cluster mass deriving from this double  $\beta$  model based on the best-fit values of  $T_1 = 2.0$  keV and  $T_2 = 11.5$  keV by Böhringer et al. (1998) is shown in Fig.2. While the shape of the resulting mass profile seems to be consistent with the weak lensing result, the double  $\beta$  model with the above temperature data has significantly underestimated the cluster mass as compared with the weak lensing analysis. Next, we treat the two temperatures  $T_1$  and  $T_2$  as free parameters and search for  $(T_1, T_2)$  that give rise to the best fit of the derived cluster mass from the double  $\beta$  model to the weak lensing result. This yields  $T_1 = 4.32$  keV and  $T_2 = 20.0$  keV for the narrow and extended components, respectively, with a reduced  $\chi^2/\nu$  value of 2.38. Interestingly, these best-fit temperatures for the narrow and extended components are consistent with the reported value of  $\sim 4$  keV in the central region of the cluster inside  $\sim 0.5$  Mpc (Böhringer et al. 1998) and the cooling flow corrected value  $23.09 \pm 35.12$  keV (White 2000), respectively. We have also displayed in Fig.2 the projected mass profiles derived from other two models for  $S_x$ : (1) a single  $\beta$  model and (2) a single  $\beta$  model plus a Gaussian peak. For these two models we use an isothermal plasma of  $T = 9.0$  keV, a value obtained from the ASCA spectra within a radius of 1.7 Mpc (Böhringer et al. 1998). The goodness of the fits of the resulting cluster masses to the weak lensing measurement reads  $\chi^2/\nu = 3.55$  and 4.63 for models (1) and (2), respectively. In a similar

way to the above analysis for the double  $\beta$  model, we have performed the  $\chi^2$  fits of the projected cluster masses given by models (1) and (2) to the weak lensing determined mass profile by treating the temperature as a free parameter. It turns out that the best-fit values of temperature for the two models are  $T = 8.74$  keV with  $\chi^2/\nu = 3.48$  and  $T = 9.15$  keV with  $\chi^2/\nu = 4.59$ , respectively. These values are well within the ROSAT and ASCA spectral measurements. It is likely that the double  $\beta$  model fit gives the smallest  $\chi^2$  value, and thus provides the most precise description for the intracluster gas, although the current fit is still unsatisfactory. Nevertheless, it should be pointed out that the measurement uncertainties in the fitting of  $S_x$  and the spectral measurement of temperature have not been included in the final mass estimate of the cluster. In particular, using a double  $\beta$  model instead of a single  $\beta$  model will lead to a large uncertainty in the derived cluster mass since the central surface brightness, core radius and  $\beta$  parameter in a double  $\beta$  model fit cannot be well constrained at present. Finally, as compared with the single  $\beta$  model, the double  $\beta$  model results in a significantly large cluster mass within small radii ( $\sim 100$  kpc), and the overall dark matter distribution clearly exhibits two distinct length scales. Similar result has also been reported in previous studies (e.g. Ikebe et al. 1996). However, it is unlikely that the central mass excess as a result of the employment of the double  $\beta$  model can resolve the mass discrepancy between the strong lensing and X-ray measurements (Wu & Fang 1997), despite the fact that our fitted core radius ( $r_{c2} = 0.035 \pm 0.005$  Mpc) is relatively small. Our result agrees with the recent analysis by Lewis et al. (1999), who found the X-ray mass within the arc radius is 2.3 times smaller than the value reported by Allen (1998),  $2.1 \times 10^{14} M_\odot$ . This indicates again that the previously claimed mass discrepancy between strong lensing and other methods has probably arisen from the oversimplification of lensing model for matter distribution in the central cores of the strong lensing clusters.

#### 4 THE $\beta$ DISCREPANCY

In this section we discuss whether the well-known puzzle, the so-called  $\beta$  discrepancy (e.g. Bahcall & Lubin 1994), may have also arisen from the employment of the conventional  $\beta$  model for intracluster gas. Briefly, if both galaxies and gas are the tracers of the depth and shape of a common gravitational potential of a cluster, we would expect the following identity (Cavaliere & Fusco-Femiano 1976; Bahcall & Lubin 1994)

$$\beta_{spec} \equiv \frac{\sigma^2}{kT/\mu m_p} = \frac{d \ln n_{gas}/d \ln r}{d \ln n_{gal}/d \ln r} \equiv \beta_{fit}, \quad (23)$$

where  $\sigma$  is the velocity dispersion of galaxies, and the number densities of galaxies and gas are denoted by  $n_{gal}$  and  $n_{gas}$ , respectively. For simplicity, we have assumed an isotropic and isothermal matter distribution for the cluster. The  $\beta$  discrepancy arises from a statistical estimate of  $\beta_{spec}$  and  $\beta_{fit}$ , which turns out that on average  $\beta_{spec}$  ( $\approx 1$ ) is larger than  $\beta_{fit}$  ( $\approx 2/3$ ). Basically, two solutions to the puzzle have so far been suggested: Either the galaxy profile in clusters may be less steeper than the simplified King model, or the present X-ray and optical observations have

only probed some finite regions of clusters so that the asymptotic value of  $\beta_{fit}$  has not yet been reached (Gerbal, Durret & Lachièze-Rey 1994).

Numerical studies of cluster formation and evolution (e.g. Navarro, Frenk & White 1995; Lewis et al. 1999) have shown that the gas density profiles of clusters become steeper with radius and therefore, a larger  $\beta$  value can be obtained if the fit to the observed X-ray surface brightness profile is extended to large radii. Indeed, Vikhlinin et al. (1999) have tried a single  $\beta$  model fit to the gas distribution in the outer regions of clusters between 0.3 and 1 virial radius. They found that the typical  $\beta$  values among the 39 clusters observed by ROSAT PSPC would be larger by  $\approx 0.05$  than that derived from the global fit. These results provide a useful clue to our reconsideration of the  $\beta$  discrepancy because only the asymptotic  $\beta$  value at large radii is of significance for the evaluation of  $\beta_{fit}$ . As has been pointed out in the above section, the  $\beta$  parameters for the two components of a double  $\beta$  model may both become larger than the value in a single  $\beta$  model fit. Replacing the  $\beta$  in eq.(23) by the  $\beta$  parameter of the extended component of a double  $\beta$  model may give rise to a larger value of  $\beta_{fit}$ . Hence, this opens a new possibility of reconciling  $\beta_{spec}$  with  $\beta_{fit}$ .

#### 4.1 CLUSTER SAMPLE

We begin with the sample of 45 ROSAT PSPC observed nearby clusters compiled recently by MME. We choose this sample because MME have already tried a double  $\beta$  model fit to the 18 clusters of their sample, which can be used for the purpose of comparison, although their double  $\beta$  model assumed the same  $\beta$  parameter for the two components. In order to estimate  $\beta_{spec}$ , we exclude those clusters whose velocity dispersion and temperature are not observationally determined. This reduces the MME sample to 33 clusters (see Table 1 and Table 2). We reanalyze the archival ROSAT PSPC imaging data of the 33 clusters following the same procedure of MME, who binned the X-ray surface brightness according to photon counts. We have also tried to measure  $S_x(r)$  using the concentric rings of equal width (1 arcminute) but found that the data points are too few for some clusters. To facilitate the double  $\beta$  model fit to  $S_x(r)$ , we will use the results of  $S_x(r)$  from MME.

We fit the observed X-ray surface brightness of clusters to a double  $\beta$  model described by eq.(6). We employ the Monte Carlo simulations and the  $\chi^2$ -fit to obtain the best-fit parameters ( $S_{0i}$ ,  $r_{ci}$ ,  $\beta_i$ ) and estimate their error bars, in which we keep the same outer radii of the fitting regions as those defined by MME. Essentially, the fitting can be classified as two types, and a typical example for each type is displayed in Fig.3. In the first case which is applied to 15 clusters in Table 1, the narrow component contributes mainly to the central X-ray emission and exhibits a sharp drop at large radii, while the extended component dominates the emission in the outer region. As for our example A2052 in Fig.3, a single  $\beta$  model fit gives  $\beta = 0.593 \pm 0.050$  but the minimum  $\chi^2$  is 310.67 for 49 d.o.f. Our double  $\beta$  fit yields  $\beta_1 = 0.810 \pm 0.194$  and  $\beta_2 = 0.773 \pm 0.029$  with  $\chi^2/\nu = 60.67/46$ . It appears that our best-fit  $\beta$  parameter for the extended component is comparable to the one (0.712) found by MME using a double  $\beta$  model fit with the same  $\beta$  parameter for the two components. In the second case, the

central emission is similarly governed by the narrow component. However, the narrow component exhibits a flatter slope than the extended component does in the outer region. Yet, the amplitude of the narrow component is significantly smaller than that of the extended component. We will thus take a less vigorous approach to the selection of the  $\beta$  parameter: The value of the extended component will be used in our evaluation of  $\beta_{fit}$  below. Mathematically, the fitted X-ray surface brightness profile will be eventually dominated by the narrow and shallower component at very large radii because of its smaller value of  $\beta$ . For A1060 shown in Fig.3, the minimum  $\chi^2$  of 598.3 in a single  $\beta$  model fit for 113 d.o.f. has been reduced to 139.9 in our double  $\beta$  model fit for 110 d.o.f. The best-fit  $\beta$  parameter of the extended component is  $0.732 \pm 0.065$ , in comparison with the MME result  $\beta = 0.703^{+0.044}_{-0.036}$ .

The best-fit  $\beta$  parameters by a double  $\beta$  model for our cluster sample are listed in Table 1, together with the results for a single  $\beta$  model fit, Quoted errors are 68% confidence limits. Note that the  $\beta$  values of the narrow components for about 1/3 of our clusters have not been well constrained. This is partially due to the fact that a single  $\beta$  model fit is acceptable for some clusters such as A401, A1367, A1651 and A4059. Another reason comes from the sparse data points at small radii, which makes it difficult to place a robust constraint on the narrow component.

We searched the literature for the velocity dispersion of galaxies and the temperature of X-ray emitting gas in our cluster sample (Table 2). Essentially, we take the X-ray temperature data of White (2000) (except A2244 and A3532) because the effect of the cooling flow on the cluster temperature has been corrected for. The majority of the velocity dispersion data are chosen from the substructure corrected values by Girardi et al. (1998). The  $\beta_{spec}$  value (the significance at 68% confidence) is correspondingly calculated for each cluster and listed in Table 2.

#### 4.2 THE $\beta$ PARAMETERS

The mean value of  $\beta_{spec}$  over 33 clusters in Table 2 is  $\langle\beta_{spec}\rangle = 0.78 \pm 0.37$ , which is consistent with previous findings within uncertainty [see Wu, Fang & Xu (1998) for a summary]. This value can be slightly raised to  $\langle\beta_{spec}\rangle = 0.80 \pm 0.36$  if A754 is excluded from the list. This cluster gives rise to the smallest value of  $\beta_{spec}$  because of its relatively small velocity dispersion or high temperature. Similar effect was also noticed in previous work, i.e., the mean value of  $\beta_{spec}$  can be biased high or low because of a few clusters in the sample. For instance, Bird, Mushotzky & Metzler (1995) found that their mean value of  $\beta_{spec} = 1.20$  drops to 1.09 if A2052 is removed from their cluster list. Using a large sample of 149 clusters, Wu, Fang & Xu (1998) showed  $\langle\beta_{spec}\rangle = 1.00 \pm 0.49$  but the median value is only  $\langle\beta_{spec}\rangle = 0.80^{+1.04}_{-0.52}$ .

The mean values of  $\beta_{fit}$  (we will assume a simplified King model for galaxy number density profile) from Table 1 are  $\langle\beta_{fit}\rangle = 0.61 \pm 0.09$  and  $\langle\beta_{fit}\rangle = 0.83 \pm 0.33$  for a single and double  $\beta$  fit, respectively. While the error bar is still large, the value of  $\langle\beta_{fit}\rangle$  has been apparently increased in the case of a double  $\beta$  model fit to  $S_x(r)$ . For comparison, the mean value of  $\beta_{fit}$  in the MME sample is  $\langle\beta_{fit}\rangle = 0.61$  for a single  $\beta$  model fit among 27 clusters, while  $\langle\beta_{fit}\rangle = 0.70$

**Table 1.** Cluster Sample:  $\beta_{fit}$ 

cluster	$\beta^a$	$\beta_1^b$	$\beta_2^c$	$\beta_{MME}^d$
A85	0.579 ± 0.009	0.975 ± 0.305	0.687 ± 0.010	0.662
A262	0.447 ± 0.004	0.542 ± 0.169	0.575 ± 0.045	0.556
A401	0.612 ± 0.006	1.016 ± 1.05	0.679 ± 0.040	0.606
A426	0.548 ± 0.007	0.688 ± 0.045	1.156 ± 0.132	0.748
A478	0.661 ± 0.008	0.723 ± 0.242	0.736 ± 0.041	0.713
A496	0.544 ± 0.008	0.734 ± 0.218	0.708 ± 0.034	0.650
A754	0.761 ± 0.025	1.01 ± 0.26	1.60 ± 0.11	0.614
A1060	0.587 ± 0.012	0.601 ± 0.326	0.732 ± 0.065	0.703
A1367	0.766 ± 0.023	0.785 ± 0.671	1.554 ± 0.731	0.707
A1651	0.637 ± 0.013	1.22 ± 1.76	0.705 ± 0.019	0.616
A1656	0.683 ± 0.048	0.504 ± 0.090	0.851 ± 0.131	0.705
A1689	0.752 ± 0.026	1.25 ± 0.07	0.954 ± 0.040	0.648
A1795	0.652 ± 0.010	1.01 ± 0.146	0.691 ± 0.040	0.790
A2029	0.637 ± 0.010	0.746 ± 0.178	0.833 ± 0.071	0.705
A2052	0.564 ± 0.005	0.810 ± 0.194	0.773 ± 0.029	0.712
A2063	0.576 ± 0.010	1.10 ± 0.97	0.658 ± 0.014	0.706
A2142	0.656 ± 0.010	1.305 ± 1.139	0.786 ± 0.037	0.787
A2199	0.611 ± 0.003	0.631 ± 0.209	0.679 ± 0.040	0.663
A2244	0.580 ± 0.017	0.846 ± 0.617	0.644 ± 0.283	0.594
A2256	0.822 ± 0.016	0.348 ± 0.030	0.926 ± 0.031	0.792
A2319	0.578 ± 0.009	0.840 ± 0.995	0.745 ± 0.059	0.828
A3112	0.568 ± 0.003	0.735 ± 0.155	0.535 ± 0.014	0.562
A3266	0.795 ± 0.024	2.09 ± 3.17	1.07 ± 0.05	0.744
A3391	0.510 ± 0.016	0.355 ± 0.038	0.704 ± 0.275	0.541
A3526	0.464 ± 0.006	0.531 ± 0.051	0.824 ± 0.169	0.569
A3532	0.598 ± 0.023	0.471 ± 0.233	0.783 ± 0.425	0.589
A3562	0.488 ± 0.004	0.610 ± 0.578	0.551 ± 0.039	0.470
A3571	0.645 ± 0.011	0.822 ± 0.652	0.795 ± 0.061	0.610
A3667	0.598 ± 0.014	0.864 ± 0.317	1.26 ± 0.35	0.541
A4059	0.603 ± 0.013	0.790 ± 0.734	0.740 ± 0.033	0.558
AWM7	0.600 ± 0.013	0.518 ± 0.058	0.801 ± 0.070	0.678
Cygnus-A	0.470 ± 0.006	0.587 ± 0.048	0.902 ± 0.618	0.472
MKW3s	0.598 ± 0.009	1.16 ± 1.79	0.645 ± 0.017	0.562
Average	0.613 ± 0.090	0.819 ± 0.400	0.833 ± 0.334	0.648

<sup>a</sup>The single  $\beta$  model;<sup>b</sup>Narrow component in the double  $\beta$  model;<sup>c</sup>Extended component in the double  $\beta$  model;<sup>d</sup>The best-fit  $\beta$  parameter by MME. Error bars are not listed.

for a double  $\beta$  model fit for the rest 18 clusters. Recall that their double  $\beta$  model assumed the same  $\beta$  parameter for the two components. Our result of  $\beta_{fit}$  for a single  $\beta$  model is in good agreement with the one found by MME. However, our double  $\beta$  model fit yields a slightly larger mean value of  $\beta_{fit}$ , which is nevertheless consistent with the claim ( $0.84 \pm 0.1$ ) by Bahcall & Lubin (1994) (Note the different definition of  $\beta_{fit}$ ), and in particular with the numerical result ( $0.82 \pm 0.06$ ) by Navarro et al. (1995).

We now examine whether the observationally fitted parameter  $\beta_{fit}$  in the outer regions of clusters have any dependence on temperature or velocity dispersion. Fig.4 shows the best-fit  $\beta_{fit}$  versus  $T$  for our cluster sample. We fit the data points to an expression  $\beta_{fit} = (T/\text{keV})^a + b$ , and find  $(a, b) = (0.17 \pm 0.03, -0.73 \pm 0.05)$  and  $(a, b) = (0.22 \pm 0.03, -0.71 \pm 0.08)$  for a single and double  $\beta$  model fit, respectively. We thus confirm the claim by Vikhlinin et

al. (1999) that  $\beta_{fit}$  has a mild trend to increase with temperature, although we get somewhat a larger variation of  $\beta_{fit}$  from  $\beta_{fit} \approx 0.56$  (0.48) for  $T = 3$  keV to  $\approx 0.93$  (0.75) for  $T = 10$  keV in a double (single) model fit.

We then study the distribution of  $\beta_{spec}/\beta_{fit}$  for each cluster, aiming at examining whether the spectroscopic parameter  $\beta_{spec}$  correlates with the observationally fitted parameter  $\beta_{fit}$  from  $S_x(r)$ . To this end, we display in Fig.5  $\beta_{spec}$  against  $\beta_{fit}$  for our 33 clusters. Indeed, there is a positive correlation between the two  $\beta$  parameters. A  $\chi^2$  fit excluding the data point of A754 yields  $\beta_{spec} = 10^{0.018 \pm 0.044} \beta_{fit}^{1.12 \pm 0.29}$ , indicating that a high  $\beta_{fit}$  corresponds to a high  $\beta_{spec}$ . Moreover, the above relation is also consistent with  $\beta_{spec} = \beta_{fit}$ , although the mean values of  $\beta_{spec}$  and  $\beta_{fit}$  are on average smaller than unity (see below).

Finally, we examine whether there is a  $\beta$  discrepancy

**Table 2.** Cluster Sample:  $\beta_{spec}$ 

cluster	$\sigma$ (km s <sup>-1</sup> )	$T$ (keV)	$\beta_{spec}$
A85	969 <sup>+95</sup> <sub>-61</sub> a	6.74 <sup>+0.50</sup> <sub>-0.50</sub> b	0.850 <sup>+0.257</sup> <sub>-0.155</sub>
A262	525 <sup>+47</sup> <sub>-33</sub> a	2.29 <sup>+0.12</sup> <sub>-0.09</sub> b	0.734 <sup>+0.173</sup> <sub>-0.121</sub>
A401	1152 <sup>+86</sup> <sub>-70</sub> a	10.68 <sup>+1.11</sup> <sub>-0.94</sub> b	0.758 <sup>+0.202</sup> <sub>-0.152</sub>
A426	1026 <sup>+106</sup> <sub>-64</sub> a	7.71 <sup>+0.29</sup> <sub>-0.37</sub> b	0.833 <sup>+0.232</sup> <sub>-0.127</sub>
A478	904 <sup>+261</sup> <sub>-140</sub> c	7.42 <sup>+0.71</sup> <sub>-0.54</sub> b	0.672 <sup>+0.531</sup> <sub>-0.234</sub>
A496	687 <sup>+89</sup> <sub>-76</sub> a	4.51 <sup>+0.17</sup> <sub>-0.15</sub> b	0.638 <sup>+0.204</sup> <sub>-0.152</sub>
A754	662 <sup>+77</sup> <sub>-50</sub> a	12.85 <sup>+1.77</sup> <sub>-1.35</sub> b	0.208 <sup>+0.082</sup> <sub>-0.052</sub>
A1060	610 <sup>+52</sup> <sub>-43</sub> a	3.27 <sup>+0.11</sup> <sub>-0.09</sub> b	0.694 <sup>+0.146</sup> <sub>-0.114</sub>
A1367	822 <sup>+88</sup> <sub>-72</sub> c	3.99 <sup>+0.48</sup> <sub>-0.48</sub> b	1.033 <sup>+0.406</sup> <sub>-0.265</sub>
A1651	965 <sup>+160</sup> <sub>-107</sub> c	7.15 <sup>+0.84</sup> <sub>-0.62</sub> b	0.794 <sup>+0.388</sup> <sub>-0.232</sub>
A1656	821 <sup>+49</sup> <sub>-38</sub> c	10.03 <sup>+0.89</sup> <sub>-0.81</sub> b	0.410 <sup>+0.091</sup> <sub>-0.067</sub>
A1689	1470 <sup>+210</sup> <sub>-160</sub> d	9.48 <sup>+1.36</sup> <sub>-0.52</sub> b	1.3901 <sup>+0.531</sup> <sub>-0.425</sub>
A1795	834 <sup>+85</sup> <sub>-76</sub> a	7.26 <sup>+0.51</sup> <sub>-0.40</sub> b	0.584 <sup>+0.167</sup> <sub>-0.133</sub>
A2029	1164 <sup>+98</sup> <sub>-78</sub> a	8.22 <sup>+0.58</sup> <sub>-0.20</sub> b	1.005 <sup>+0.203</sup> <sub>-0.188</sub>
A2052	714 <sup>+143</sup> <sub>-148</sub> e	3.30 <sup>+0.16</sup> <sub>-0.13</sub> b	0.942 <sup>+0.471</sup> <sub>-0.377</sub>
A2063	667 <sup>+55</sup> <sub>-41</sub> a	3.90 <sup>+0.51</sup> <sub>-0.38</sub> b	0.696 <sup>+0.207</sup> <sub>-0.154</sub>
A2142	1132 <sup>+110</sup> <sub>-92</sub> a	10.96 <sup>+2.56</sup> <sub>-1.58</sub> b	0.713 <sup>+0.290</sup> <sub>-0.225</sub>
A2199	801 <sup>+92</sup> <sub>-61</sub> a	4.70 <sup>+0.13</sup> <sub>-0.15</sub> b	0.833 <sup>+0.236</sup> <sub>-0.141</sub>
A2244	1204 <sup>+232</sup> <sub>-86</sub> f	8.47 <sup>+0.43</sup> <sub>-0.42</sub> g	1.044 <sup>+0.518</sup> <sub>-0.396</sub>
A2256	1348 <sup>+86</sup> <sub>-64</sub> a	8.69 <sup>+1.06</sup> <sub>-1.06</sub> b	1.275 <sup>+0.368</sup> <sub>-0.244</sub>
A2319	1545 <sup>+95</sup> <sub>-77</sub> a	13.60 <sup>+2.22</sup> <sub>-2.22</sub> b	1.070 <sup>+0.371</sup> <sub>-0.240</sub>
A3112	552 <sup>+86</sup> <sub>-63</sub> h	4.69 <sup>+0.27</sup> <sub>-0.26</sub> b	0.396 <sup>+0.164</sup> <sub>-0.102</sub>
A3266	1107 <sup>+82</sup> <sub>-65</sub> a	9.69 <sup>+0.97</sup> <sub>-0.92</sub> b	0.771 <sup>+0.212</sup> <sub>-0.150</sub>
A3391	663 <sup>+195</sup> <sub>-112</sub> a	6.90 <sup>+1.47</sup> <sub>-0.86</sub> b	0.389 <sup>+0.355</sup> <sub>-0.167</sub>
A3526	780 <sup>+100</sup> <sub>-100</sub> e	4.04 <sup>+0.11</sup> <sub>-0.11</sub> b	0.918 <sup>+0.283</sup> <sub>-0.239</sub>
A3532	738 <sup>+112</sup> <sub>-85</sub> a	4.4 <sup>+4.7</sup> <sub>-1.3</sub> i	0.755 <sup>+0.667</sup> <sub>-0.469</sub>
A3562	736 <sup>+49</sup> <sub>-36</sub> a	6.96 <sup>+1.77</sup> <sub>-0.95</sub> b	0.475 <sup>+0.151</sup> <sub>-0.132</sub>
A3571	1045 <sup>+109</sup> <sub>-90</sub> a	8.12 <sup>+0.42</sup> <sub>-0.39</sub> b	0.820 <sup>+0.230</sup> <sub>-0.169</sub>
A3667	1045 <sup>+62</sup> <sub>-47</sub> a	8.11 <sup>+0.82</sup> <sub>-0.73</sub> b	0.709 <sup>+0.172</sup> <sub>-0.126</sub>
A4059	845 <sup>+280</sup> <sub>-140</sub> j	4.05 <sup>+0.23</sup> <sub>-0.19</sub> b	1.075 <sup>+0.924</sup> <sub>-0.367</sub>
AWM7	864 <sup>+110</sup> <sub>-80</sub> a	3.96 <sup>+0.16</sup> <sub>-0.14</sub> b	1.150 <sup>+0.365</sup> <sub>-0.240</sub>
Cygnus-A	1581 <sup>+286</sup> <sub>-197</sub> k	39.40 <sup>+2.66</sup> <sub>-2.66</sub> b	0.387 <sup>+0.192</sup> <sub>-0.109</sub>
MKW3s	610 <sup>+69</sup> <sub>-52</sub> a	3.71 <sup>+0.16</sup> <sub>-0.19</sub> b	0.612 <sup>+0.187</sup> <sub>-0.121</sub>
Average	925 ± 281	7.86 ± 6.36	0.777 ± 0.367

References.– (a)Girardi et al. 1998; (b)White 2000; (c)Zabludoff et al. 1990; (d)Jones & Forman 1999; (e)Bird et al. 1995; (f)Struble & Rood 1991; (g)Mushotzky & Scharf 1997; (h)Fadda et al. 1996; (i)Edge et al. 1990; (j)Green et al. 1988; (k)Owen et al. 1997.

for clusters. we plot in Fig.6 the ratio of  $\beta_{spec}$  to  $\beta_{fit}$  for each cluster in our cluster sample. For a single  $\beta$  model, the mean ratio is  $\langle \beta_{spec}/\beta_{fit} \rangle = 1.28 \pm 0.41$ , while for a double  $\beta$  model, this value becomes  $\langle \beta_{spec}/\beta_{fit} \rangle = 0.99 \pm 0.35$ . Therefore, it seems that there is no apparent  $\beta$  discrepancy for clusters within the framework of a double  $\beta$  model fit to  $S_x(r)$ .

## 5 DISCUSSION AND CONCLUSIONS

The conventional  $\beta$  model appears to be inaccurate, and the extrapolation of a single  $\beta$  model to large radii could be misleading. The monotonic increase of baryon fraction with radius and the so-called  $\beta$  discrepancy, together with the

luminosity divergence as a result of the too small  $\beta_{fit}$  parameters ( $\beta_{fit} \leq 1/2$ ) for some clusters, may have a common origin: A single  $\beta$  model fit to the entire regions of the X-ray surface brightness profiles of clusters yields an underestimate of  $\beta_{fit}$  parameter at large radii. The exclusion of the central data points or the employment of a double  $\beta$  model in the fitting of the observed X-ray surface brightness profiles can lead to an apparent increase of  $\beta_{fit}$  at large radii, which may allow one to resolve all the puzzles mentioned above, although these two empirical methods both depend on the extent of the fitting regions. Yet, in the conventional treatment the cooling flow regions are often excluded from the  $\beta$  model fit, which may suffer from the uncertainty of different strategies of choice of the cutoff radii (e.g. Jones

& Forman 1984; White, Jones & Forman 1997; Vikhlinin, Forman & Jones 1999). As a result, the accuracy of our determination of the total cluster mass from X-ray measurements may be correspondingly affected. Employing the second  $\beta$  model to quantitatively describe the central excess X-ray emission can significantly improve the goodness of the fit, which thus enables us to derive more accurately the gas and total dynamical masses of clusters. In the present paper, we have extensively studied the properties of a double  $\beta$  model, and demonstrated its applications using two examples: A2597 and A2390. In particular, as compared with a single  $\beta$  model, a double  $\beta$  model via the hydrostatic equilibrium hypothesis for intracluster gas gives rise to a larger X-ray cluster mass at the central region, although this correction is still insufficient to resolve the discrepancy between the strong lensing and X-ray determined cluster masses enclosed within the arc radius (e.g. Wu et al. 1998). It is hoped that the mathematical treatments of a double  $\beta$  model developed in the present paper will be useful for future work.

The  $\beta$  parameter as an indicator of the dynamical properties of clusters discussed in the present paper and the baryon fraction of clusters as an indicator of cosmological matter composition discussed in literature (White et al. 1993; David, Jones & Forman 1995; Wu & Xue 2000 and references therein) concern mainly the asymptotic behavior of clusters at large radii, while a double  $\beta$  model provides a more precise way to describe the variation of intracluster gas at large radii. We have thus studied the possibility of resolving the well-known  $\beta$  discrepancy using a double model fit to the X-ray surface brightness of clusters. We have found, based a sample of 33 clusters drawn from a recent catalog of MME, that the spectroscopic parameter  $\beta_{spec}$  is on average consistent with the observationally fitted parameter  $\beta_{fit}$  from the X-ray surface brightness profile.

Of course, the definite resolution to the  $\beta$  discrepancy also needs a better understanding of the distributions of cluster galaxies and their velocity dispersion at large radii (Bahcall & Lubin 1994; Girardi et al. 1996), for which we have assumed a simplified King model with a constant and isotropic velocity dispersion in the present paper. A shallower galaxy density profile (e.g.  $n_{gal} \propto r^{-2.4}$ ) can give rise to a higher value of  $\beta_{fit}$ . Alternatively, the second X-ray core radius will become larger in a double  $\beta$  model fit. In our cluster sample, the mean core radii of the narrow and extended components are  $\langle r_{c1} \rangle = 0.14 \pm 0.14$  Mpc and  $\langle r_{c1} \rangle = 0.48 \pm 0.38$  Mpc, respectively. Since the extended component is involved in the evaluation of  $\beta_{fit}$ , a good approximation of  $\beta_{fit}$  can only be achieved at very large radii. So, the effect of finite observational sizes may cause another uncertainty, and the extension of the fitting region will lead to an increase of  $\beta_{fit}$ . As a whole, these two effects, the shallower galaxy density profile and the extension of the X-ray fitting region, can both result in a high  $\beta_{fit}$ . Therefore, it is possible that the  $\beta$  discrepancy still remains but  $\beta_{fit} > \beta_{spec}$ .

Finally, within the framework of energy equipartition the ratio of kinetic energy in the galaxies to that in the gas should be close to unity. Although our estimate of  $\langle \beta_{spec} \rangle = 0.78 \pm 0.37$  is still consistent with such a prediction within the error bars, this value, together with the consistent  $\beta_{fit}$  parameter  $\langle \beta_{fit} \rangle = 0.83 \pm 0.33$ , does not exclude the possibility that the actual value of  $\langle \beta_{spec} \rangle$  is smaller than

1, namely,  $\langle \sigma^2 \rangle < \langle kT \rangle / \mu m_p$ . Here, we will not intend to explore in detail the physical mechanisms for the scenario. However, we would like to point out that the dynamical friction would resist the motion of galaxies in clusters, leading to a velocity dispersion smaller than that expected from the purely dissipationless hypothesis (e.g. Carlberg & Dubinski 1991; Metzler & Evrard 1994). This may account for our result – why galaxies appear to be cooler than intracluster gas.

## ACKNOWLEDGMENTS

We thank Haiguang Xu for useful discussion and help with the understanding of the ROSAT PSPC data reduction, and an anonymous referee for many valuable suggestions and comments. This work was supported by the National Science Foundation of China, under Grant No. 1972531.

## REFERENCES

- Allen S. W., 1998, MNRAS, 296, 392  
 Bahcall N. A., Lubin L.M., 1994, ApJ, 426, 513  
 Bird C. M., Mushotzky R. F., Metzler C. A., 1995, ApJ, 453, 40  
 Böhringer H., Tanaka Y., Mushotzky R. F., Ikebe Y., Hattori M., 1998, A&A, 334, 789  
 Buote D., 2000, MNRAS, 311, 176  
 Cavaliere A., Fusco-Femiano R., 1976, A&A, 49, 137  
 Carlberg R. G., Dubinski J., 1991, ApJ, 369, 13  
 Cowie L. L., Henriksen M., Mushotzky R. F., 1987, ApJ, 317, 593  
 David L. P., Jones C., Forman W., 1995, ApJ, 445, 578  
 Edge A. C., Stewart G. C., Fabian A. C., Arnaud K. A., 1990, MNRAS, 245, 559  
 Fadda D., Girardi M., Giuricin G., Mardirossian F., Mezzetti M., 1996, ApJ, 473, 670  
 Gerbal D., Durret F., Lachièze-Rey M., 1994, A&A, 288, 746  
 Girardi M., Fadda D., Giuricin G., Mardirossian F., Mezzetti M., Biviano A., 1996, ApJ, 457, 61  
 Girardi M., Giuricin G., Mardirossian F., Mezzetti M., Boschin W., 1998, ApJ, 505, 74  
 Green M. R., Godwin J. G., Peach J. V., 1988, MNRAS, 234, 1051  
 Gunn K. F., Thomas P. A., 1996, MNRAS, 281, 1133  
 Henry J. P., Henriksen M. J., 1986, ApJ, 301, 689  
 Ikebe Y., et al., 1996, Nature, 379, 427  
 Ikebe Y., Makishima K., Fukazawa Y., Tamura T., Xu H., Ohashi T., Matsushita K., 1999, ApJ, 525, 581  
 Jones C., Forman W., 1984, ApJ, 276, 38  
 Jones C., Forman W., 1999, ApJ, 511, 65  
 Lewis G. F., Babul A., Katz N., Quinn T., Hernquist L., Weinberg D. H., 1999, ApJ, submitted (astro-ph/9907097)  
 Lewis A. D., Ellingson E., Morris S. L., Carlberg R. G., 1999, ApJ, 517, 587  
 Makino N., Sasaki S., Suto Y., 1998, ApJ, 497, 55  
 Metzler C. A., Evrard A. E., 1994, ApJ, 437, 564  
 Mohr J. J., Mathiesen B., Evrard A. E., 1999, ApJ, 517, 627 (MME)  
 Mushotzky R. F., Scharf C. A., 1997, ApJ, 482, L13  
 Nagai D., Sulkanen M. E., Evrard A. E., 2000, MNRAS, submitted (astro-ph/9903308)  
 Navarro J. F., Frenk C. S., White S. D. M., 1995, MNRAS, 275, 720  
 Nulsen P. E. J., 1986, MNRAS, 221, 377  
 Owen F. N., Ledlow M. J., Morrison G. E., Hill J. M., 1997, ApJ, 488, L15



- Reiprich T. H., Böhringer H., 1999, preprint (astro-ph/9909071)
- Rizza E., Burns J. O., Ledlow M. J., Owen F. N., Voges W., Bliton M., 1998, MNRAS, 301, 328
- Sarazin C. L., McNamara B. R., 1997, ApJ, 408, 203
- Squires G., Kaiser N., Babul A., Fahlman G., Woods D., Neumann D. M., Böhringer H., 1996, ApJ, 461, 572
- Struble M. F., Rood H. J., 1991, ApJS, 77, 363
- Vikhlinin A., Forman W., Jones, C., 1999, ApJ, 525, 47
- White D. A., 2000, MNRAS, 312, 663
- White D. A., Fabian A. C., 1995, MNRAS, 273, 72
- White D. A., Jones C., Forman W., 1997, MNRAS, 292, 419
- White S. D. M., Navarro J. F., Evrard A. E., Frenk C. S., 1993, Nature, 366, 429
- Wu X.-P., Chiueh T., Fang L.-Z., Xue Y.-J., 1998, MNRAS, 301, 861
- Wu X.-P., Fang L.-Z., 1997, ApJ, 483, 62
- Wu X.-P., Fang L.-Z., Xu W., 1998, A&A, 339, 813
- Wu X.-P., Xue Y.-J., 2000, MNRAS, 311, 825
- Xu H., et al., 1998, ApJ, 500, 738
- Zabludoff A. I., Huchra J. P., Geller M. J., 1990, ApJS, 74, 1

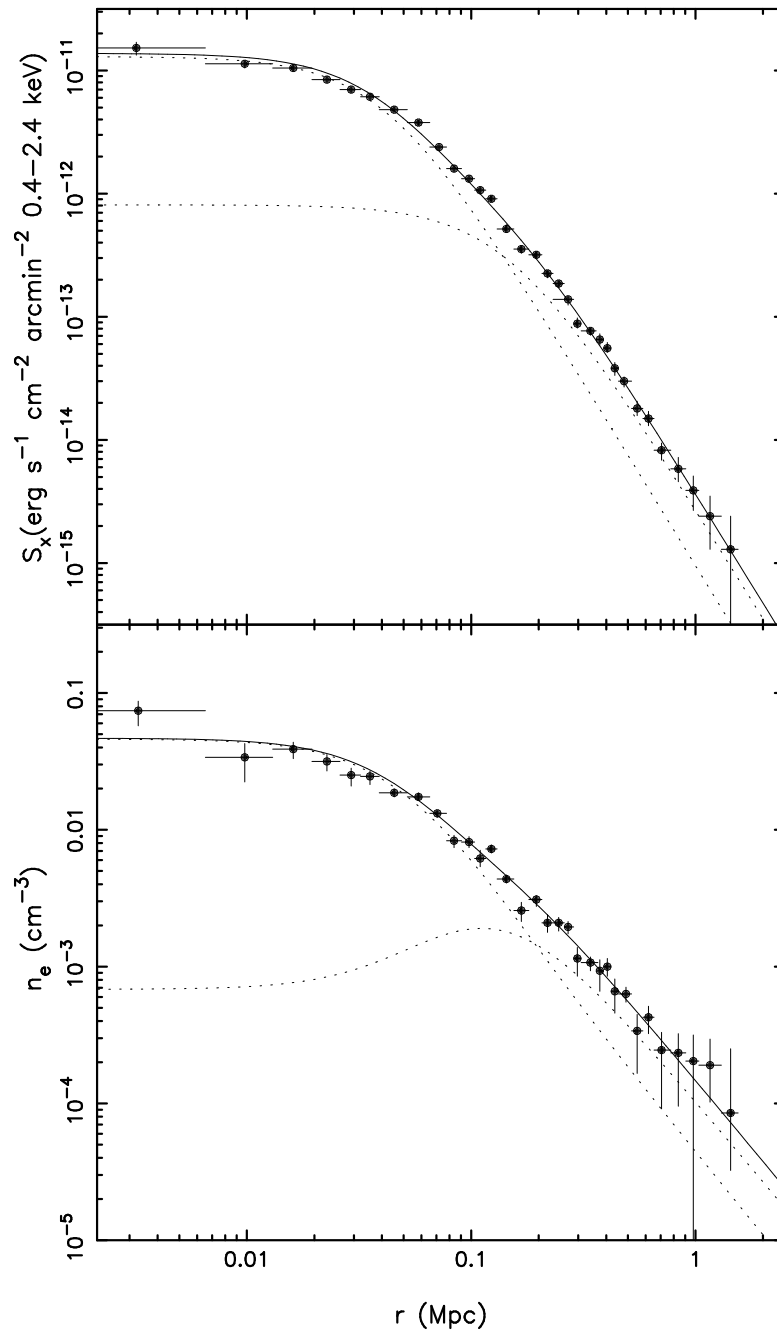


**Figure 1.** Upper panel: The merged ROSAT HRI and PSPC surface brightness profile for A2579 (Sarazin & McNamara 1997), along with the best-fit double  $\beta$  model (solid line). The effect of the PSF of the ROSAT HRI has been corrected. Lower panel: A comparison of the electron number density derived from the deprojection technique (Sarazin & McNamara 1997) and that from the best-fit double  $\beta$  model (solid line). The dotted lines represent the two components of the double  $\beta$  model.

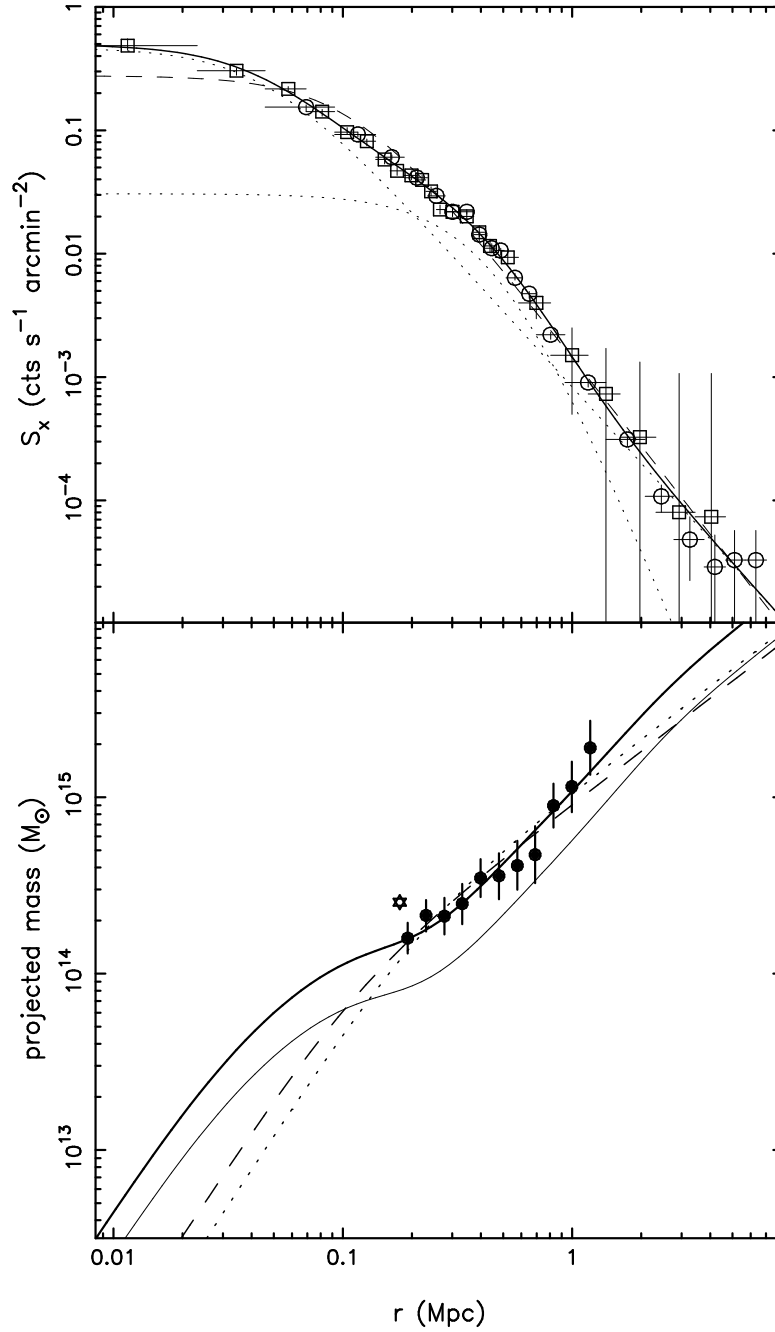


**Figure 2.** Upper panel: The superimposed ROSAT HRI (squares) and PSPC (circles) surface brightness profiles for A2390 (Böhringer et al. 1998). Also plotted are the best-fit double  $\beta$  model (solid line) and the best-fit single  $\beta$  model (dashed line) for the entire data points. The dotted lines represent the two components of the double  $\beta$  model. Lower panel: A comparison of the projected cluster masses revealed by weak gravitational lensing (filled circles) (Squires et al. 1996) and by the X-ray measurements via hydrostatic equilibrium hypothesis: thin solid line – the best-fit double  $\beta$  model with  $T_1 = 2$  keV and  $T_2 = 11.5$  keV; thick solid line – the best-fit double  $\beta$  model with  $T_1 = 4.32$  keV and  $T_2 = 20.0$  keV; dashed line – the best-fit single  $\beta$  model for the entire data points; dotted line – the single  $\beta$  model fit by exclusion of the central emission excess. The strong lensing derived cluster mass is also shown by asterisk (Wu et al. 1998).

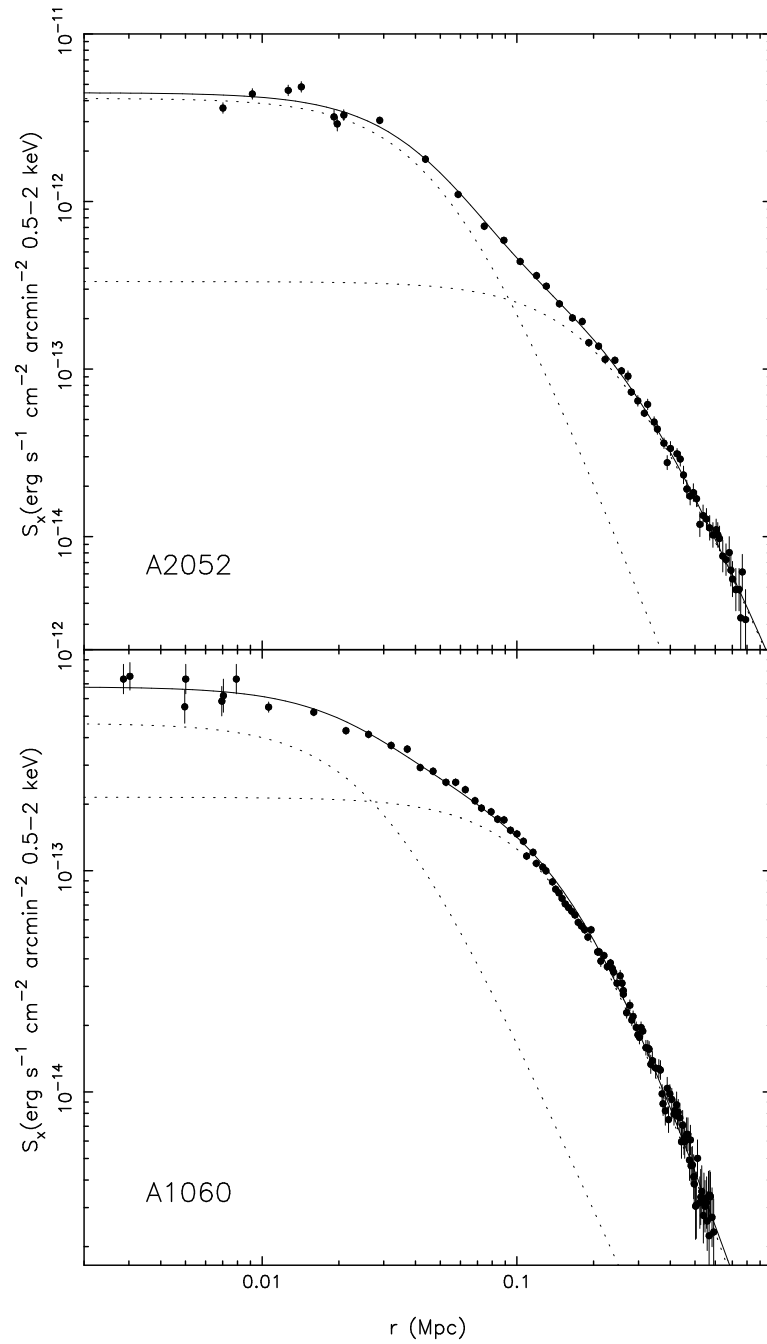


**Figure 3.** Two typical examples of the ROSAT PSPC observed and the double  $\beta$  model fitted surface brightness profiles, A2052 and A1060. The dotted lines represent the two components of the double  $\beta$  model.

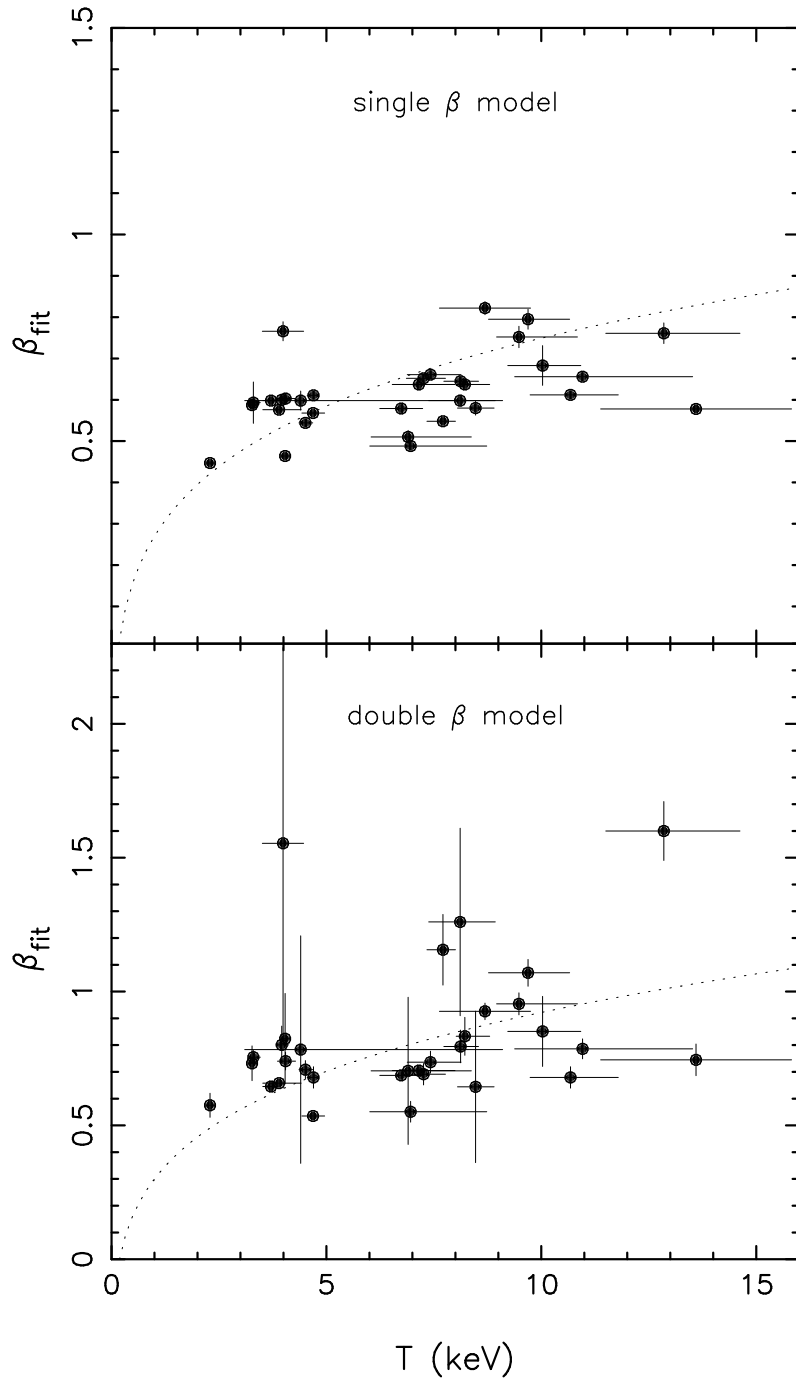


**Figure 4.** The  $\beta$  parameters obtained from a single (upper panel) and double (lower panel)  $\beta$  model fit plotted against the X-ray temperature. The dotted lines are the best-fit correlations represented by the form  $\beta = T^a + b$ , in which  $a = 0.17 \pm 0.03$  and  $0.22 \pm 0.03$  for a single and double  $\beta$  model, respectively. Cygnus-A is not shown in the plot due to its high temperature (39.40 keV).

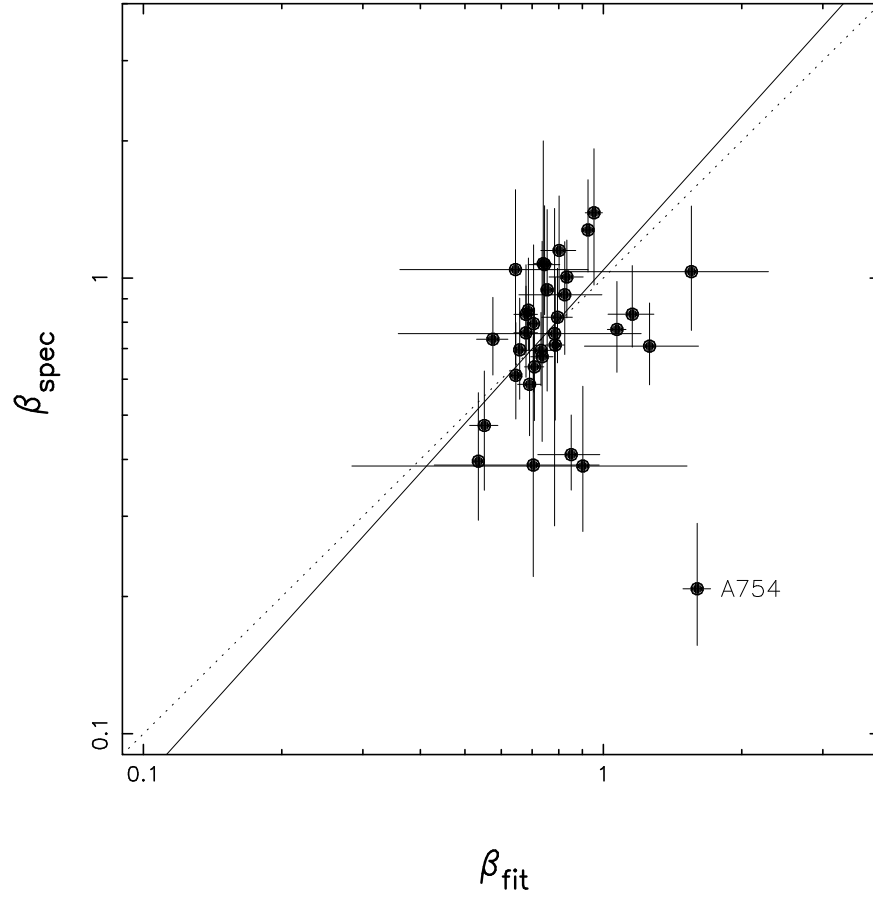


**Figure 5.** The spectroscopic parameter  $\beta_{spec}$  is plotted against the observationally fitted parameter  $\beta_{fit}$  from  $S_x(r)$  for our sample of 33 clusters. The solid line is the best  $\chi^2$ -fit power-law relation to the data set with exclusion of A754:  $\beta_{spec} \propto \beta_{fit}^{1.12}$ , while the dotted line denotes  $\beta_{spec} = \beta_{fit}$ .

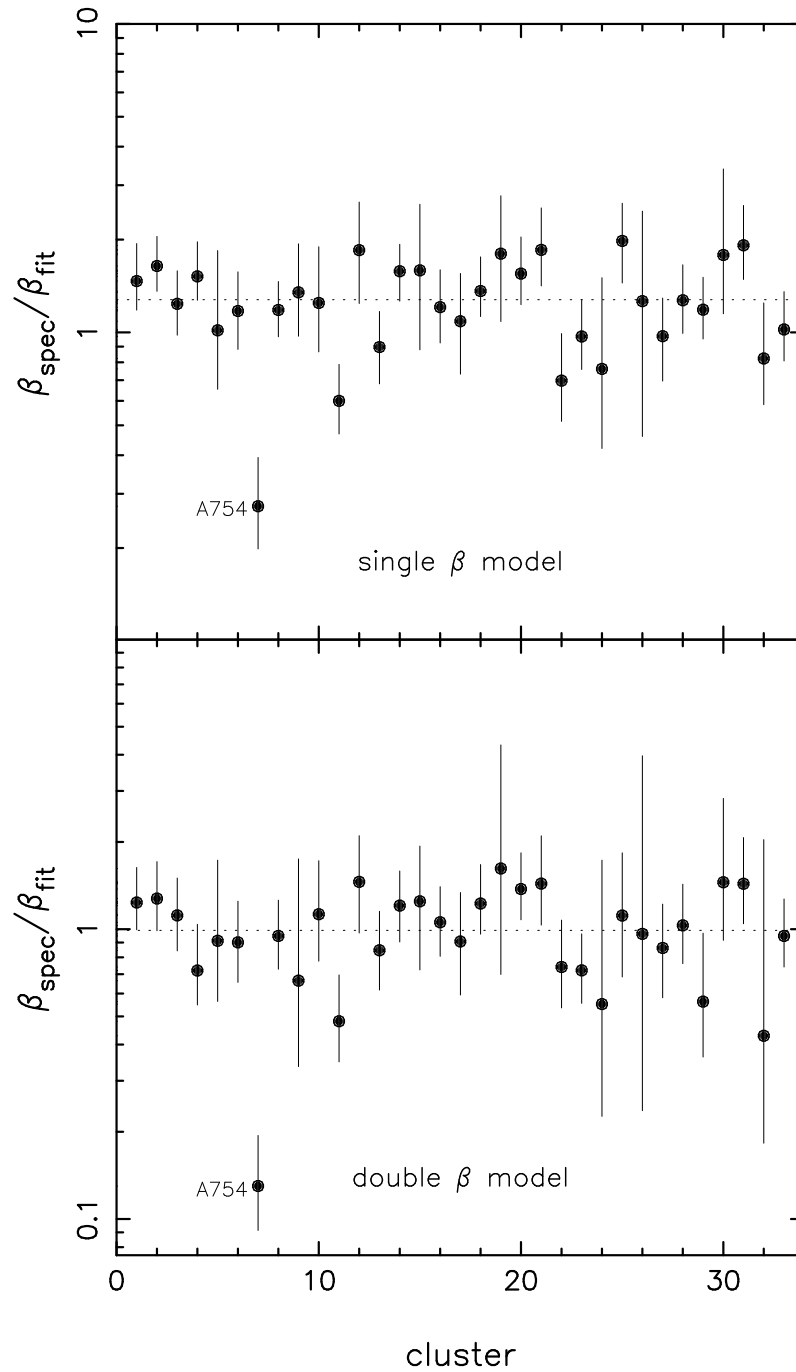


**Figure 6.** The ratio of  $\beta_{\text{spec}}$  to  $\beta_{\text{fit}}$  for an ensemble of 33 clusters. Upper and lower panels correspond to a single and double  $\beta$  model fit, respectively. The dotted lines denote the mean ratios.